Metabolism Clinical and Experimental 88 (2018) 1–11

Contents lists available at ScienceDirect

Metabolism Clinical and Experimental

journal homepage: www.metabolismjournal.com

Basic Science

Liver-specific ablation of insulin-degrading enzyme causes hepatic insulin resistance and glucose intolerance, without affecting insulin clearance in mice

Pablo Villa-Pérez [a], Beatriz Merino [a], Cristina M. Fernández-Díaz [a], Pilar Cidad [a], Carmen D. Lobatón [a], Alfredo Moreno [a], Harrison T. Muturi [b,e], Hilda E. Ghadieh [b,e], Sonia M. Najjar [b,e], Malcolm A. Leissring [c], Irene Cózar-Castellano [a], Germán Perdomo [d,*]

[a] Instituto de Biología y Genética Molecular, University of Valladolid-CSIC, Valladolid, Spain
[b] Department of Biomedical Sciences, Ohio University, USA
[c] Institute for Memory Impairments and Neurological Disorders, University of California, UCI MIND, Irvine, CA, USA
[d] Departamento de Ciencias de la Salud, Universidad de Burgos, Burgos, Spain
[e] Diabetes Institute, Heritage College of Osteopathic Medicine, Ohio University, USA

ARTICLE INFO

Article history:
Received 23 March 2018
Accepted 6 August 2018

Keywords:
Insulin-degrading enzyme
Hepatic insulin resistance
Insulin receptor
Carcinoembryonic antigen-related cell adhesion molecule 1

ABSTRACT

The role of insulin-degrading enzyme (IDE), a metalloprotease with high affinity for insulin, in insulin clearance remains poorly understood. OBJECTIVE: This study aimed to clarify whether IDE is a major mediator of insulin clearance, and to define its role in the etiology of hepatic insulin resistance.
Methods: We generated mice with liver-specific deletion of *Ide* (L-IDE-KO) and assessed insulin clearance and action.
Results: L-IDE-KO mice exhibited higher (~20%) fasting and non-fasting plasma glucose levels, glucose intolerance and insulin resistance. This phenotype was associated with ~30% lower plasma membrane insulin receptor levels in liver, as well as ~55% reduction in insulin-stimulated phosphorylation of the insulin receptor, and its downstream signaling molecules, AKT1 and AKT2 (reduced by ~40%). In addition, FoxO1 was aberrantly distributed in cellular nuclei, in parallel with up-regulation of the gluconeogenic genes *Pck1* and *G6pc*. Surprisingly, L-IDE-KO mice showed similar plasma insulin levels and hepatic insulin clearance as control mice, despite reduced phosphorylation of the carcinoembryonic antigen-related cell adhesion molecule 1, which upon its insulin-stimulated phosphorylation, promotes receptor-mediated insulin uptake to be degraded.
Conclusion: IDE is not a rate-limiting regulator of plasma insulin levels in vivo.

1. Introduction

Insulin-degrading enzyme (IDE) is a 110-kDa zinc-metalloendopeptidase first identified and named based on its ability to bind to and degrade insulin [1]. IDE also degrades several other intermediate-sized (<80 amino acids) bioactive peptides, including glucagon, amylin and the amyloid β-protein [2]. IDE is ubiquitously expressed at varying levels in both insulin-responsive and -nonresponsive cell types. Subcellularly, the protease is primarily cytosolic, but it has been reported to exist within a number of intracellular vesicles, and organelles, as well as being associated with membranes, and secreted into the extracellular space [1,3–6]. This wide distribution suggests a dynamic and multifunctional role for IDE.

Because IDE has a high affinity for insulin (K_M = ~100 nM), it has been proposed as the major enzyme responsible for its catabolism [3,7]. In vivo, insulin is produced and secreted by pancreatic β-cells, which is delivered through the portal venous system to the liver, where it is primarily cleared, although kidneys and other tissues also degrade the hormone [1]. In first-pass transit, the liver removes ~50% of circulating insulin. Although the detailed molecular mechanisms of hepatic insulin clearance are not fully understood, insulin uptake and intracellular degradation is a receptor-mediated process that occurs after the binding of the hormone to its receptor (IR) [8]. The insulin-IR complex is endocytosed via clathrin-coated vesicles and is primarily delivered to endosomes. In the acidic milieu of the endosomes, insulin dissociates from the IR, at which point insulin is believed to be degraded by IDE, and the receptor is recycled back to the plasma membrane [1]. In recent years, a role for the carcinoembryonic antigen-related cell adhesion molecule 1 (CEACAM1) in promoting receptor-mediated insulin uptake has emerged [9]. Upon its phosphorylation by the receptor, CEACAM1 binds to and increases the rate of the

* Corresponding author at: Universidad de Burgos, Facultad de Ciencias de la Salud, Departamento de Ciencias de la Salud, P.O. Comendadores s/n (Antiguo Hospital Militar), 09001 Burgos, Spain.
E-mail address: gmperdomo@ubu.es (G. Perdomo).

https://doi.org/10.1016/j.metabol.2018.08.001

insulin-receptor complex uptake to be targeted to the cellular degradation pathways, contributing to the regulation of systemic insulin concentrations [10].

The physiological role of IDE in insulin clearance in vivo began to be clarified with the study of mice with global null mutation of *Ide* (IDE-KO mice). Consistent with a functional role for IDE in hepatic insulin clearance, IDE-KO mice exhibit chronic hyperinsulinemia resulting from impaired insulin clearance [11,12]. They also exhibit marked glucose intolerance and insulin resistance [11,12]. These results spurred the notion that transient and/or partial inhibition of IDE may represent a new pharmacological approach against type 2 diabetes (T2DM) [11,13,14]. However, pharmacological inhibition of IDE in mice caused contradictory observations regarding glucose homeostasis [15–17]. Furthermore, genetic polymorphisms within or near the *Ide* locus have been linked to increased, rather than decreased, risk for T2DM [18–22].

Therefore, the role of IDE in insulin clearance, and how this may modulate insulin resistance remain to be clarified. To address these questions, we ablated *Ide* expression exclusively in hepatocytes, the major site of insulin clearance, and investigated its effect on insulin clearance and action.

2. Material and Methods

2.1. Mice Generation and Genotyping

Mice were fed standard rodent chow diet and water ad libitum in ventilated cages under a 12:12-h light-dark cycle at the animal facility of the University of Valladolid (UVa). L-IDE-KO mice were generated from crosses between the B6.Cg-Tg(Alb-cre)21Mgn/J mouse (*Alb-Cre* mouse (The Jackson Laboratory, USA) that expresses *Cre* recombinase cDNA from the mouse albumin (*Alb*) promoter [23], and the *Ide* $^{flox/flox}$ mouse on the C57BL/6 J (B6) background (from Dr. Malcolm A. Leissring, University of California, Irvine). This mouse has *loxP* sites flanking *exon 3* of the *Ide* gene. *Cre* recombinase-mediated deletion of *exon 3* causes a frameshift with two stop codons in *exon 4* and early termination of translation. Twenty-three independent cohorts (males and females) of the F3 generation were used for metabolic studies and tissue collection. The IDE-KO mice were kindly provided by Dr. Malcolm A. Leissring [11]. The Animal Care and Use Committee of the UVa approved all experiments (protocol #5003931).

The *Alb-Cre+* control mice did not show abnormal metabolic phenotype relative to the C57BL/6J mice that were used in backcrossing. As Supplementary Table 1 reveals, *Alb-Cre+* controls manifested comparable body weight and visceral obesity to that of C57BL/6J, in addition to normoinsulinemia and normal insulin clearance (measured by steady-state molar ratio of C-peptide/insulin levels). These control mice also showed normal insulin and glucose tolerance by comparison to C57BL/6J mice (Supplementary Fig. 1). Thus, we only used *Ide* $^{flox/flox;}$ +/+ as wildtype (WT) controls in these studies.

Mice genotyping was performed using genomic DNA isolated from mouse tail as described previously [24], followed by three PCRs to amplify: *gapdh*, *Ide* and *Alb-Cre* genes. Breeding strategy and genotyping of mice are detailed in the Supplementary Experimental Procedures.

2.2. Plasma Biochemistry

Fasting (16 h) and non-fasting (fed ad libitum) blood glucose and plasma triglycerides levels were assessed as described previously [24]. Plasma mouse insulin and glucagon levels were assessed using human or mouse enzyme-linked immunosorbent (ELISA) assays following the manufacturer's instructions (Mercodia, Sweden). Plasma amylin (Phoenix Pharmaceutical, USA) and amyloid (Aβ40) (Invitrogen, USA) levels by ELISA assays following the manufacturer's instructions. Plasma C-peptide levels were assessed by ELISA (ALPCO, USA).

2.3. Hepatic Triglycerides and Glycogen Levels

Hepatic triglyceride content was assessed as described previously by Perdomo et al. [25]. Liver glycogen content was assessed using the Glycogen Assay Kit (Sigma-Aldrich, USA). Briefly, liver samples (10 mg) were homogenized in 100 μL of water supplemented with protease and phosphatase inhibitor cocktails (Sigma-Aldrich, USA) on ice. Homogenates were boiled at 100 °C for 5 min to inactivate enzymes and centrifuged 5 min at 12300 ×*g* at room temperature to remove insoluble materials. Homogenates were diluted 1:100 in hydrolysis buffer up to a final volume of 50 μL and mixed with 2 μL of Hydrolysis Enzyme Mix for 30 min at room temperature. Glycogen concentration was determined by a coupled enzyme assay, which yields a colorimetric (570 nm) product, proportional to the glycogen present in the homogenate.

2.4. Metabolic Studies

To evaluate alterations in glucose homeostasis in vivo, we performed intraperitoneal glucose tolerance tests (IP-GTTs) and insulin tolerance tests (IP-ITTs) as described previously [26]. In vivo plasma insulin clearance was performed as described by Ahrén et al. [27] with some modifications. Briefly, 3-month-old mice were fasted for 2 h, then anesthetized using a solution of medetomidine plus ketamine at 0,125 mg/100 g body weight. Afterwards, human insulin (Humulin; Lilly, USA) was injected intra-orbitally at 1 nmol/kg and blood samples were collected from the tail vein 0, 5, 10, 20, 30 and 60 min after insulin administration. Plasma human insulin levels were quantified using a human ELISA kit (Mercodia, Sweden) following the manufacturer's instructions.

2.5. Quantitative Real-time PCR

Total RNA from homogenized mouse tissues was isolated using Trizol Reagent (Sigma-Aldrich, USA) following the manufacturer's protocol. After DNAse treatment 500–1000 ng of RNA was used to synthesize

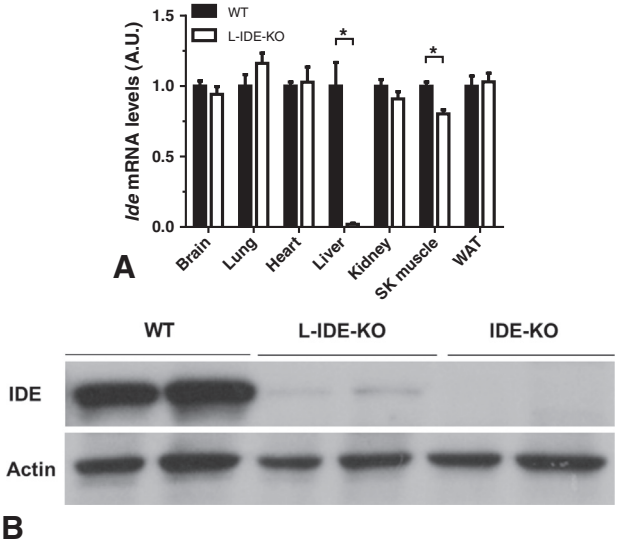

Fig. 1. Analysis of IDE expression in WT and L-IDE-KO mice. **(A)** Expression of *Ide* mRNA in 3-month-old male L-IDE-KO and control littermates. Expression levels are mean ± SEM. $n = 4$ per genotype. *p value <0.05 vs. WT by Students' t-test. **(B)** Hepatic IDE protein levels in WT, L-IDE-KO, and IDE-KO mice. Representative western blots of liver lysates (40 μg protein/sample) isolated from 3-month-old WT, L-IDE-KO, and IDE-KO mice using anti-IDE and anti-actin antibodies. $n = 2$ per genotype.

cDNA with the Transcriptor First Strand cDNA Synthesis Kit (Roche, USA). mRNA levels were determined by real time qPCR with TaqMan® probe-based assays on a Rotor-Gene 3000 instrument (Corbett Research) using the $2^{-\Delta\Delta Ct}$ relative quantification method [28]. TaqMan® Gene Expression assay references (from Applied Biosystems, USA) were as follows: Mm00473077_m1 for *Ide*, Mm01247058_m1 for phosphoenolpyruvate carboxykinase (*Pck1*), Mm00839363_m1 for glucose-6 phosphatase (*G6pc*), Mm01211875_m1for insulin receptor (*Insr*), and Mm00802831_m1 for insulin-like growth factor-1 receptor (*Igf1r*). Expression data were normalized to the level of the housekeeping gene of the ribosomal protein L18 (RPL18; Forward: 5′-AAGACTGCCGT GGTTGTGG-3′; Reverse: 5′-AGCCTTGAGGATGCGACTC-3′; Probe: 5′-FAM-TTCCCAAGCTGAAGGTGTGTGCA-BHQ1–3′).

2.6. Western Blot Analysis

Western blot analyses on isolated mouse tissues, and subcellular localization of FoxO1 are detailed in the *Supplementary Experimental Procedures*. Rabbit anti-FoxO1 antibody was used as described by Qu et al. [29]. For co-immunoprecipitation experiments, polyclonal antibodies against Shc (B-9) was used to immunoprecipitate proteins from tissue lysates as previously described [30,31].

2.7. Analysis of β-Cell Function, Pancreatic Histology and Histomorphometry

To asses β-cell function, mice were fasted overnight followed by an i. p. injection of a bolus of glucose. Blood samples were drawn, and plasma insulin levels were measured during 30 min. as described above. Afterwards, mice were euthanized and pancreata dissected, fixed in 10% neutral buffer formalin, paraffin embedded, and sectioned as described previously [32]. For islets histomorphometry, sections were stained with anti-insulin antibody (Abcam, UK). β-cell mass, β-cell area, the number of islets, and the mean islets size were quantitated using the ImageJ software (NIH, USA) as described previously [32].

2.8. Statistical Analyses

Statistical analysis of data was performed using Prism v. 6.0 (GraphPad Software). Distributions were checked with the Kolmogorov-Smirnov test. Data are presented as means ± SEM. Comparisons between two groups were done using the unpaired Students' *t*-test. Comparisons between more than two groups were done using the one-way ANOVA (Bonferroni test for post-hoc analyses). Differences were considered significant at $p < 0.05$.

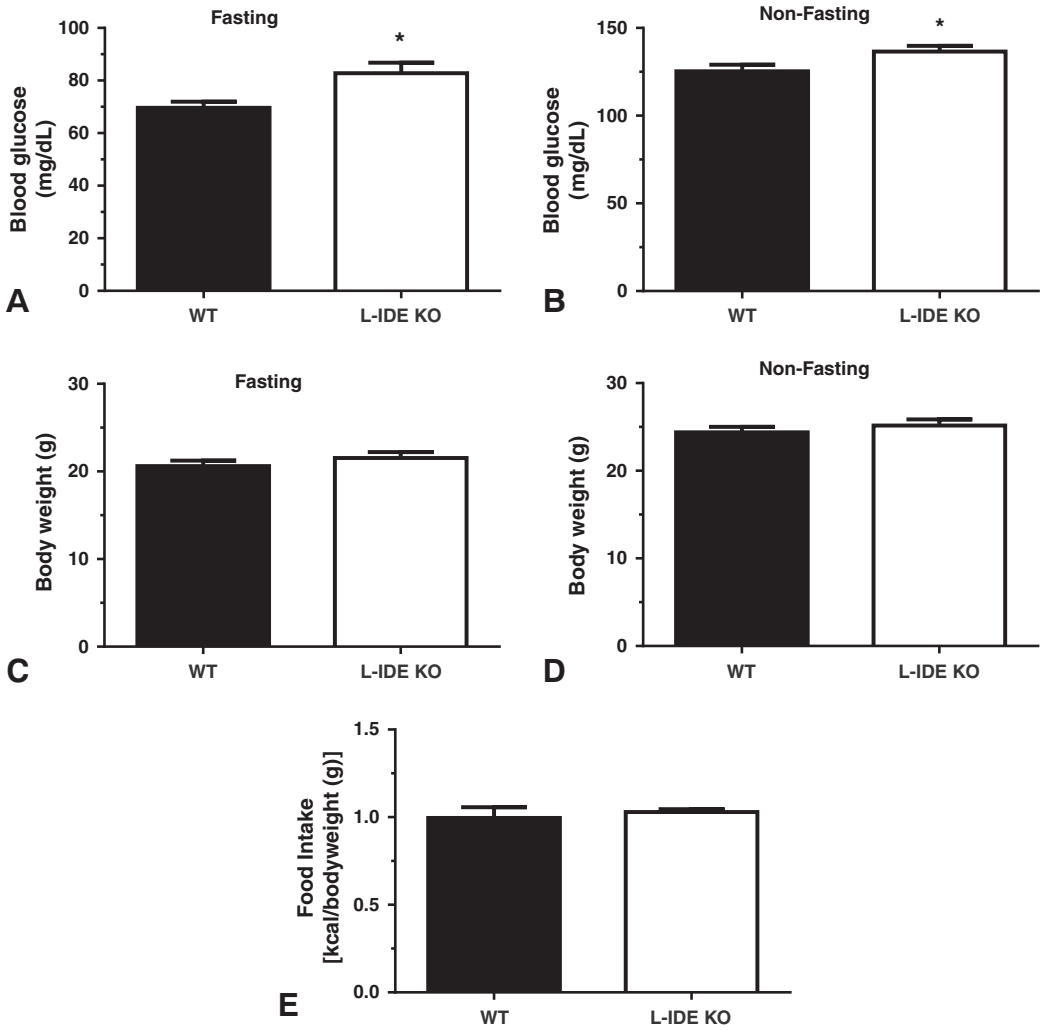

Fig. 2. Metabolic features of L-IDE-KO mice. Fasting **(A)** and non-fasting **(B)** blood glucose levels in 3-month-old male WT and L-IDE-KO mice. Data are mean ± SEM. $n = 12–13$ per genotype. $^{*}p$ value < 0.05 vs. WT by Students' *t*-test. Fasting **(C)** and non-fasting **(D)** body weight in WT and L-IDE-KO mice. Data are mean ± SEM. n = 12–13 per genotype. Food intake **(E)**. Data are mean ± SEM. $n = 5–6$ per genotype.

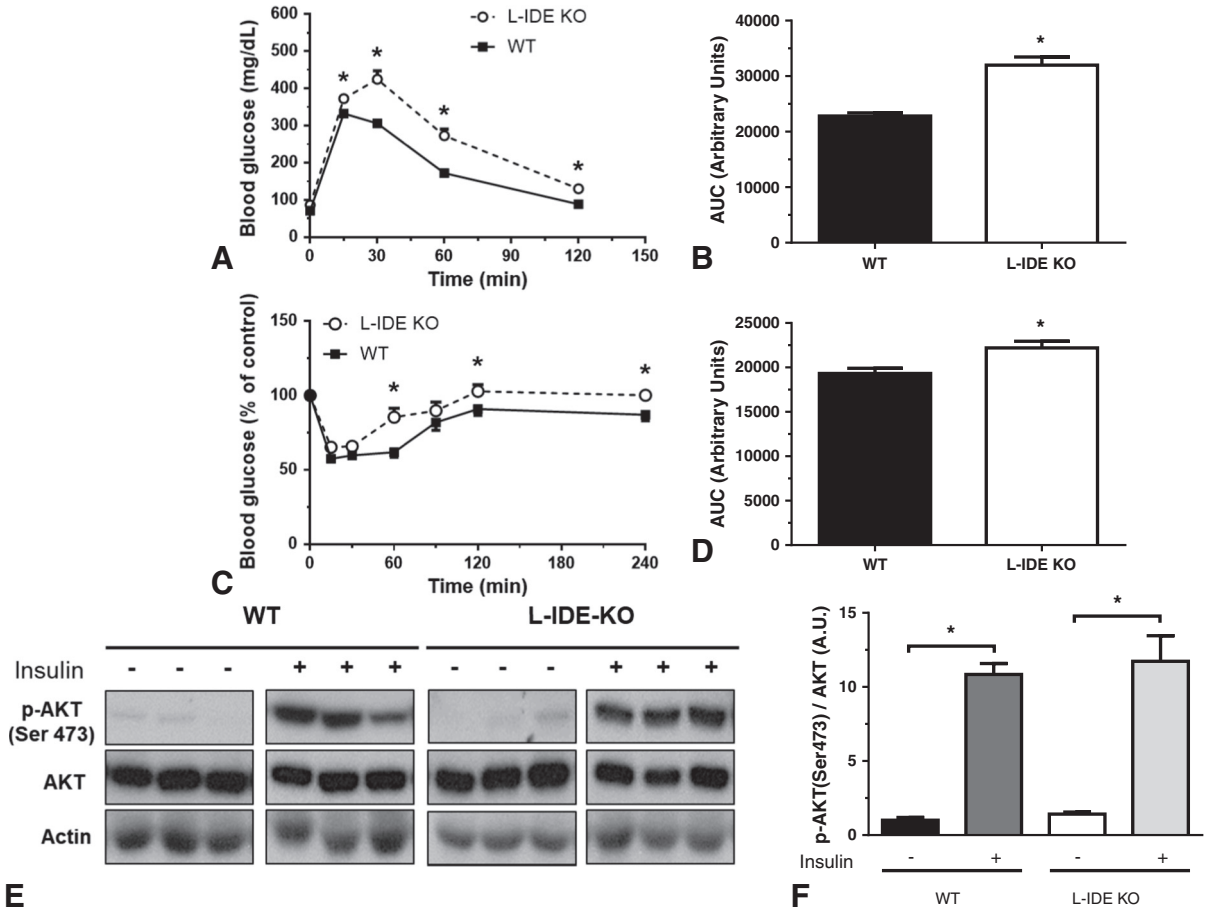

Fig. 3. L-IDE-KO mice exhibit impaired glucose homeostasis and insulin resistance. **(A)** IP-GTT of 3-month-old male mice. Data are mean ± SEM. n = 12–13 per genotype. *p value < 0.05 vs. WT by Students' t-test. **(B)** Area under the curve of the IP-GTT. *p value < 0.05 vs. WT by Students' t-test. **(C)** IP-ITT of 3-month-old male mice. Data are mean ± SEM. n = 12–13 per genotype. *p value < 0.05 vs. WT by Students' t-test. **(D)** Area under the curve of the IP-ITT. *p value < 0.05 vs. WT by Students' t-test. **(E)** Lack of effect of liver-specific IDE deletion on AKT signaling in skeletal muscle. Representative western blots depicting basal and insulin-stimulated p-AKT levels in skeletal muscle. Grouping of images from different parts of the same gel have been used for the final arrangement of the figure (see Supplementary Fig. 4 for full blots). **(F)** Densitometric analysis of Ser-473-Akt phosphorylation. The y-axis represents the ratio of phosphorylated versus total protein in arbitrary units. Data are mean ± SEM. $n = 6$ per genotype. *p value <0.05 vs. saline treatment by ANOVA.

3. Results

3.1. Generation and Molecular Characterization of Liver-specific IDE Knock-out Mice

3-month-old male and female *Ide*$^{flox/flox;}$+/+ mice (henceforth, wildtype-WT) and *Ide*$^{flox/flox;}$*Alb-Cre*/+ (L-IDE-KO) mice were studied. Hepatic *Ide* mRNA (Fig. 1A) and protein levels (Fig. 1B) were decreased by ~90–100% in L-IDE-KO mice, compared to controls. No differences in IDE expression were observed in other tissues, except for a ~20% reduction in *Ide* mRNA levels without changes in IDE protein levels in skeletal muscle (data not shown). Considering that hepatocytes make up ~85% of liver cells, it is likely that the minimal amount of IDE detected in liver of L-IDE-KO mice reflects residual expression from nonparenchymal liver cells (sinusoidal cells, endothelial, Kupffer cells, etc.) As expected, IDE-KO mice did not express IDE protein in the liver (Fig. 1B).

3.2. Hepatic IDE Deletion Leads to Glucose Intolerance and Insulin Resistance, but without Altered Insulin Metabolism

At 3 months of age, male (Fig. 2A–B) and female (Supplementary Fig. 2A–B) L-IDE-KO mice showed higher fasting and non-fasting blood glucose levels, as compared to WT controls. These changes in glucose homeostasis were not correlated with an increase in body weight (Fig. 2C–D and Supplementary Fig. 2C–D) or food intake (Fig. 2E). Consistent with this metabolic phenotype, L-IDE-KO mice exhibited glucose intolerance and insulin resistance (Fig. 3A–D and Supplementary Fig. 3). The insulin resistance observed in L-IDE-KO mice was not correlated with blunted insulin-signaling in the skeletal muscle, as shown by intact phosphorylation of protein kinase B (PKB; AKT1) in response to insulin (Fig. 3E–F).

Typically, insulin resistance is associated with hyperinsulinemia, but surprisingly, fasting and non-fasting plasma insulin levels were similar between L-IDE-KO and control mice (Fig. 4A–B; Supplementary Fig.

Fig. 4. Hepatic ablation of *Ide* does not alter plasma insulin levels and hepatic insulin clearance. Fasting **(A)** and non-fasting **(B)** plasma insulin levels in 3-month-old male WT and L-IDE-KO mice. Data are mean ± SEM. n = 12 per genotype. **(C)** Plasma insulin clearance in 3-month-old male mice. Data are mean ± SEM. $n = 9$–6 per genotype. **(D)** Area under the curve of the in vivo insulin clearance. **(E)** Fasting plasma C-peptide levels in 3-month-old mice fasted overnight. Data are mean ± SEM. n = 6–12 per genotype. **(F)** Non-fasting plasma C-peptide levels in 3-month-old mice. Data are mean ± SEM. $n = 10$–13 per genotype. **(G)** Insulin clearance was calculated as the molar ratio of C-peptide to insulin in 3-month-old mice fasted overnight. Data are mean ± SEM. $n = 6$–12 per genotype. **(H)** Non-fasting plasma glucagon levels in 3-month-old male L-IDE-KO and control littermates. Data are mean ± SEM. n = 6–9 per genotype. n.s.; nonstatistical significance. **(I)** Fasting plasma glucagon levels in 3-month-old male L-IDE-KO and control littermates. Data are mean ± SEM. n = 9 per genotype. n.s.; nonstatistical significance. **(J)** Fasting plasma amylin levels in 3-month-old male L-IDE-KO and control littermates. Data are mean ± SEM. n = 10–14 per genotype. **(K)** Fasting plasma Aβ40 levels in 3-month-old male L-IDE-KO and control littermates. Data are mean ± SEM. n = 10–15 per genotype.

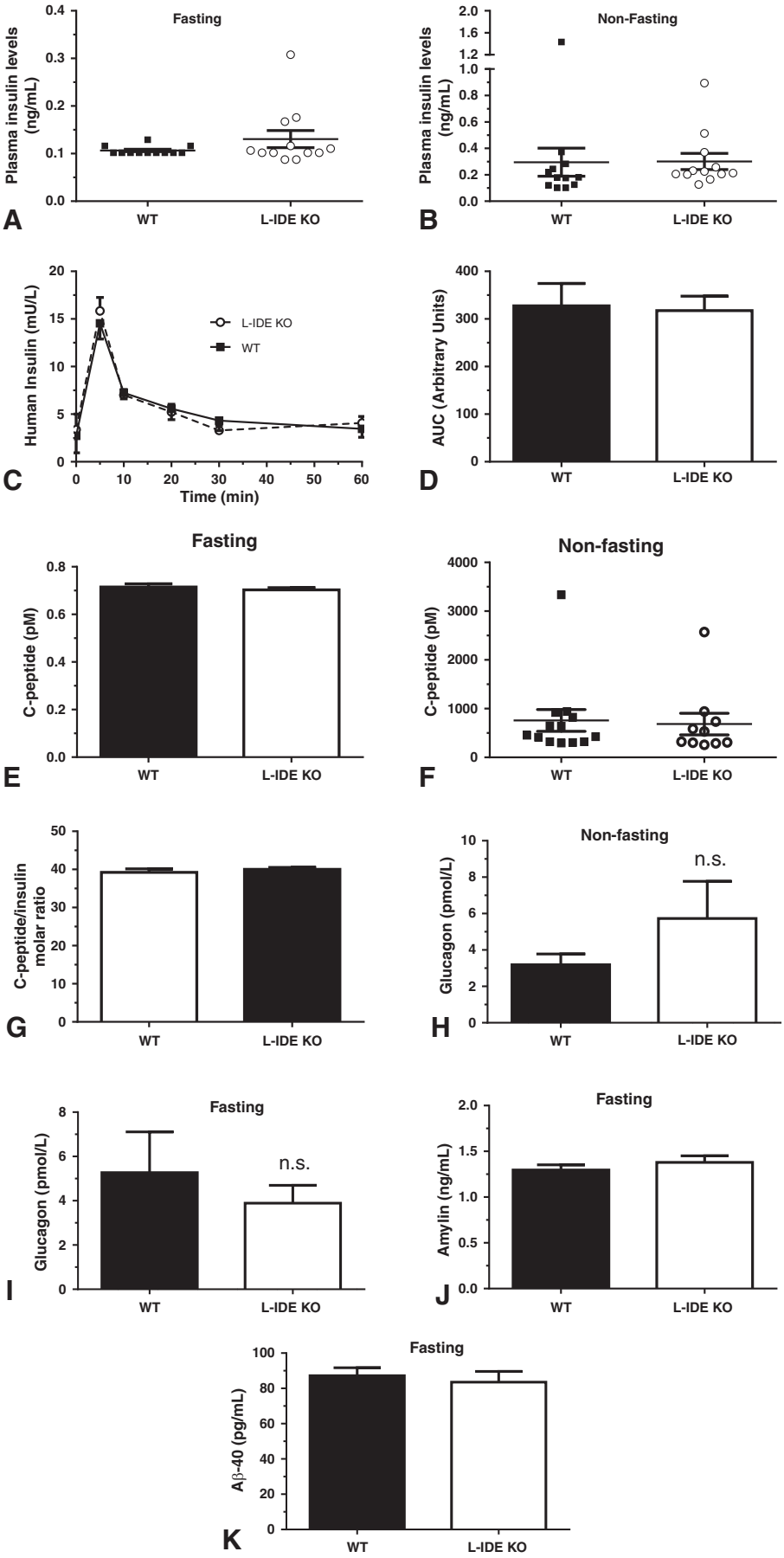
Fasting
Plasma insulin levels (ng/mL)
0.4
0.3
0.2
0.1
0.0
WT
L-IDE KO
A
Non-Fasting
Plasma insulin levels (ng/mL)
2.0
1.6
1.2
1.0
0.8
0.6
0.4
0.2
0.0
WT
L-IDE KO
B
Human Insulin (mU/L)
20
15
10
5
0
L-IDE KO
WT
0
10
20
30
40
50
60
Time (min)
C
AUC (Arbitrary Units)
400
300
200
100
0
WT
L-IDE KO
D
Fasting
C-peptide (pM)
0.8
0.6
0.4
0.2
0.0
WT
L-IDE KO
E
Non-fasting
C-peptide (pM)
4000
3000
2000
1000
0
WT
L-IDE KO
F
C-peptide/insulin molar ratio
50
40
30
20
10
0
WT
L-IDE KO
G
Non-fasting
n.s.
Glucagon (pmol/L)
10
8
6
4
2
0
WT
L-IDE KO
H
Fasting
n.s.
Glucagon (pmol/L)
8
6
4
2
0
WT
L-IDE KO
I
Fasting
Amylin (ng/mL)
2.0
1.5
1.0
0.5
0.0
WT
L-IDE KO
J
Fasting
Aβ-40 (pg/mL)
100
80
60
40
20
0
WT
L-IDE KO
K

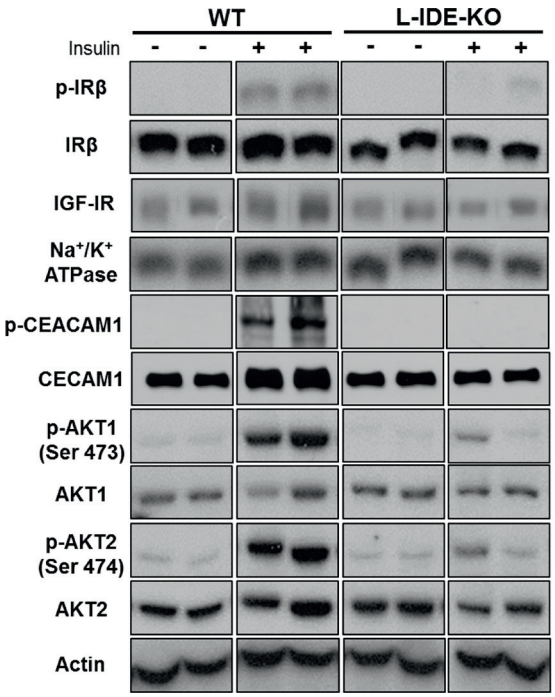
WT
L-IDE-KO
Insulin
- - + + - - + +
p-IRβ
IRβ
IGF-IR
Na+/K+ ATPase
p-CEACAM1
CECAM1
p-AKT1 (Ser 473)
AKT1
p-AKT2 (Ser 474)
AKT2
Actin

A

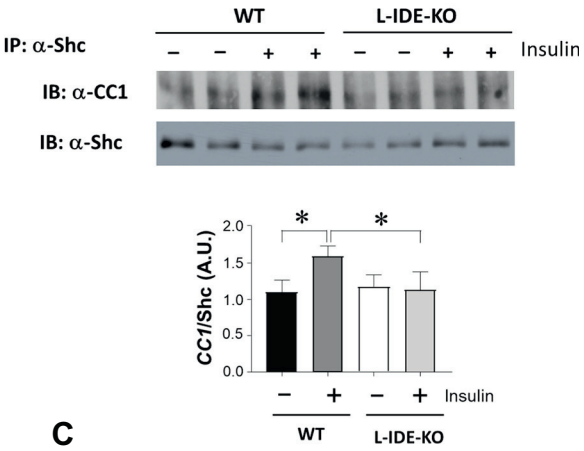
WT
L-IDE-KO
IP: α-Shc
Insulin
IB: α-CC1
IB: α-Shc
CC1/Shc (A.U.)
2.0
1.5
1.0
0.5
0.0
*
*
Insulin
WT
L-IDE-KO

C

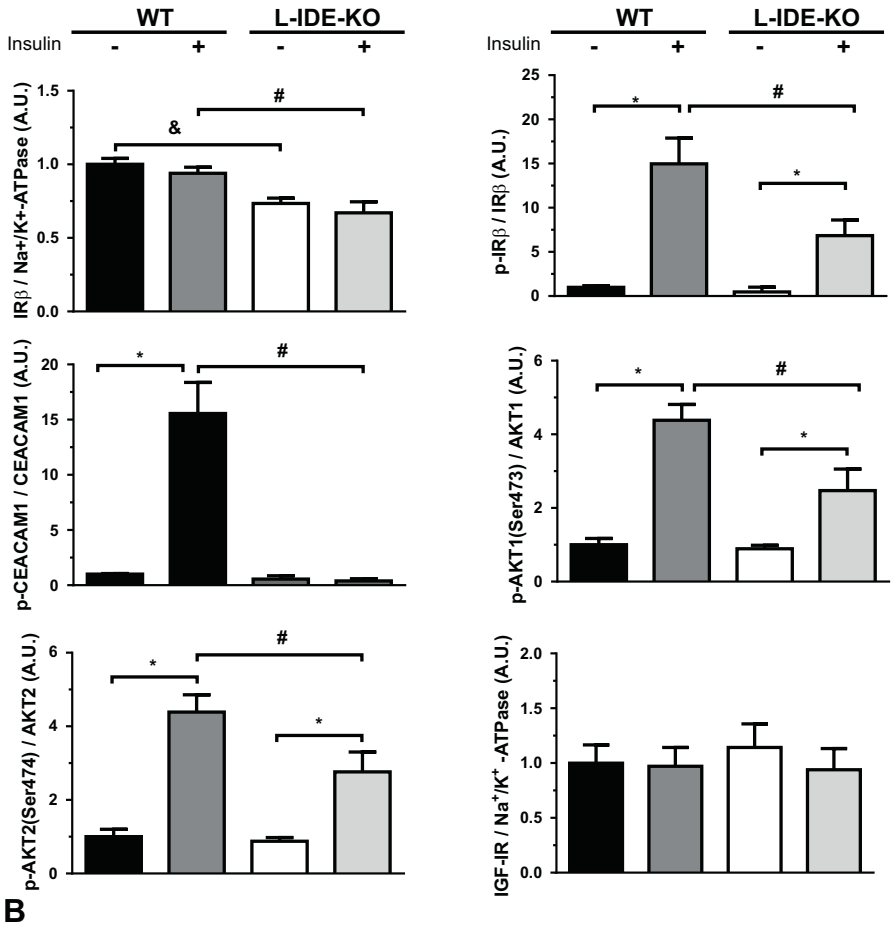
WT
L-IDE-KO
Insulin
IRβ / Na+/K+-ATPase (A.U.)
p-IRβ / IRβ (A.U.)
p-CEACAM1 / CEACAM1 (A.U.)
p-AKT1(Ser473) / AKT1 (A.U.)
p-AKT2(Ser474) / AKT2 (A.U.)
IGF-IR / Na+/K+ -ATPase (A.U.)
&
#
*

B

5A–B). These findings cast doubt on the notion that IDE is the principal protease regulating insulin catabolism in vivo [11], and that plasma insulin clearance depends on the protease activity of IDE in the liver [1]. To directly assess the role of IDE in hepatic insulin clearance, we performed an in vivo plasma insulin clearance assay. As shown in Fig. 4C–D, male L-IDE-KO mice (and female, Supplementary Fig. 5C–D) exhibited similar rates of plasma insulin clearance as controls. Likewise, insulin clearance measured as steady-state C-peptide/insulin molar ratio [10] was similar between L-IDE-KO and WT controls (Fig. 4E–G).

Like insulin, plasma glucagon, amylin and Aβ40 levels remained unchanged in L-IDE-KO as compared to WT controls (Fig. 4H–K).

3.3. IDE Is Necessary for Hepatic Insulin Signaling

To help elucidate the molecular basis underlying the insulin resistance observed in L-IDE-KO mice, we analyzed multiple components of the intracellular insulin-signaling pathway in liver tissue, a key organ involved in the regulation of whole-body glucose homeostasis. To this end, 3-month-old male L-IDE-KO and WT mice were fasted overnight, then administered an intraperitoneal injection of a bolus of insulin (0.75 U/kg) or saline solution. Ten minutes later, mice were euthanized, and tissues were dissected.

Hepatic *Ide* deletion resulted in a mild (~30%) but significant reduction of IR protein level in the plasma membrane fractions from L-IDE-KO livers, as demonstrated by Western blot analysis (Fig. 5A-B). Furthermore, its insulin-stimulated phosphorylation was reduced by ~55% in L-IDE-KO mice, compared to controls (Fig. 5A–B). Consequently, insulin-stimulated phosphorylation of its substrate, CEACAM1, was completely abolished despite no change of its hepatic basal expression by *Ide* deletion (Fig. 5A-B).

Because L-IDE-KO mice manifested a marked reduction of CEACAM1 phosphorylation in response to insulin, we hypothesized that it would be associated with changes in the internalization of the complex insulin-IR-CEACAM1. To address this question, we carried out co-immunoprecipitation experiments to detect whether deleting *Ide* affects insulin-stimulated association between Shc and CEACAM1, a critical step in the insulin's internalization process [30,33,34]. As Fig. 5C shows, immunoblotting the Shc immunopellet with CEACAM1 antibody indicated 1.5-fold increase in the Shc/CEACAM1 binding in response to insulin in the controls but not the IDE null mice.

On the other hand, the insulin-like growth factor-1 receptor (IGF-IR) exhibits 70% homology to IR, and in response to insulin shares some of the signaling pathways with the IR. Western blot analyses revealed that hepatic *Ide* deletion did not reduce IGF-IR protein levels in the plasma membrane fractions from L-IDE-KO livers (Fig. 5A-B). Likewise, *Insr* and *Igf1r* mRNA levels were similar between WT and L-IDE-KO mice in fasting and non-fasting conditions (Supplementary Fig. 7). Taken together, these results support the notion that hepatic *Ide* ablation alters posttranslational events of the IR in L-IDE-KO mice without affecting the related IGF-IR.

To further analyze downstream effects of hepatic IDE depletion on insulin signaling, we examined AKT1 and AKT2 phosphorylation in total liver lysates. AKT1 phosphorylation, which is chiefly involved in cell survival, protein synthesis and inhibition of apoptosis, and AKT2 phosphorylation, which is exclusively involved in metabolism, were both reduced, exhibiting significant reductions of ~40–45% (Fig. 5A-B).

3.4. Hepatic Ablation of IDE Causes Up-regulation of Gluconeogenic Genes

A hallmark of hepatic insulin resistance is augmented production of glucose. The forkhead box O1 (FoxO1) is a nuclear transcription factor downstream of AKT that integrates insulin signaling with gluconeogenesis in the liver, by upregulating the expression of the gluconeogenic genes *Pck1* and *G6pc* [29]. In response to insulin, FoxO1 is phosphorylated, resulting in its nuclear exclusion and inhibition of *Pck1* and *G6pc* gene expression. Hepatic insulin resistance reduces FoxO1 phosphorylation, which results in unleashed gluconeogenesis [35]. To determine whether the increased blood glucose levels observed in L-IDE-KO mice were associated with activation of gluconeogenesis, we prepared cytoplasmic and nuclear fractions of liver tissues from WT and L-IDE-KO mice treated with saline or insulin for 10 min. As shown in Fig. 6A, FoxO1 proteins were detected predominantly in the cytoplasmic fractions after stimulation with insulin in WT mice. In contrast, in L-IDE-KO mice, FoxO1 underwent a substantial subcellular redistribution, shifting from the cytoplasmic fraction to the nuclear fraction upon exposure to insulin (Fig. 6A). This was correlated with up-regulation of *Pck1* and *G6pc* mRNA expression levels under either fasting or non-fasting conditions (Fig. 6B–C).

In addition to FoxO1, AKT phosphorylates and deactivates glycogen synthase kinase 3 (GSK-3), leading to activation of glycogen synthase (GS) and thus, inducing glycogen synthesis [36]. To examine the effect of IDE depletion on glycogenesis, we quantified phosphorylation levels of GSK-3 from WT and L-IDE-KO mice treated with saline or insulin for 10 min. As Fig. 6D revels, insulin-mediated AKT phosphorylation inactivates GSK-3, which in turn restores GS activity and glycogen synthesis in WT mice. Unexpectedly, relative to WT mice, basal GSK-3 phosphorylation was 3.5-fold higher in L-IDE-KO mice and, moreover, insulin treatment failed to result in increased phosphorylation (Fig. 6D). To explore the functional impact of these perturbations, we analyzed glycogen levels in L-IDE-KO and WT livers. Surprisingly, hepatic *Ide* ablation had no effect on liver glycogen levels, under either fasting (Fig. 6E) or non-fasting (Fig. 6F) conditions. Taken together, this suggests that *Ide* deficiency in liver must result in other, as-yet unidentified mechanisms that compensate for the lack of the expected effect of AKT on GSK-3 phosphorylation and hepatic glycogen content.

Because insulin also regulates hepatic lipid metabolism via an AKT2 phosphorylation-dependent mechanism [37], we then assessed triglycerides levels in the plasma and livers of 3-month-old WT and L-IDE-KO male mice. Hepatic triglyceride content remained similar between WT and L-IDE-KO mice under either fasting (Fig. 6G) and non-fasting conditions (Fig. 6H). Similarly, circulating plasma triglycerides levels were comparable in both mouse groups regardless of the feeding status (Fig. 6I-J).

3.5. β-Cell Function and Histomorphometry in the L-IDE-KO Mice

To asses β-cell function, we monitored plasma insulin levels following an i.p. glucose injection after an overnight fasting period in WT and L-IDE-KO mice. As Fig. 7A-B shows, plasma insulin levels during IP-GTT were similar between WT and L-IDE-KO mice. Consistently, fasting and non-fasting plasma C-peptide levels remained unchanged between L-IDE-KO mice and littermate controls (Fig. 4E–F). In addition, we have assessed β-cell mass and the number of islets by histomorphometry in WT and L-IDE-KO mice. As shown in Fig. 7C–F, β-cell mass, β-cell area,

Fig. 5. Hepatic *Ide* deficiency causes multiple changes to intracellular insulin-signaling pathways. **(A)** Representative Western blots depicting the effects of insulin on total and phosphorylated IR, IGF-IR, CEACAM1, AKT1 and AKT2 levels. Expression of actin and Na^+/K^+-ATPase were determined to ensure similar protein levels for total liver lysates and lysates from liver membrane fractions (insulin receptor) respectively. Grouping of images from different parts of the same gel have been used for the final arrangement of the figure (see Supplementary Fig. 6 for full blots). **(B)** Densitometric analyses of the data in panel A. The *y*-axis represents the ratio of phosphorylated versus total protein in arbitrary units. Data are mean ± SEM. n = 6 per genotype and condition. $^{*}p$ value <0.05 vs. saline treatment by ANOVA. $^{\#}p$ value <0.05 WT + insulin vs. L-IDE-KO + insulin treatment by ANOVA. $^{\&}p$ value <0.05 WT-insulin vs. L-IDE-KO-insulin treatment by ANOVA. **(C)** Co-immunoprecipitation of CEACAM1 and Shc. Some aliquots of the above lysates used for western blotting were subjected to immunoprecipitation with α-Shc followed by immunoblotting with α-CEACAM1 antibody (α-CC1). *Upper panel*, representative image of two independent experiments with identical results. *Lower panel*, densitometric analysis of $n = 3$ independent experiments. $^{*}p$ value <0.05 by ANOVA.

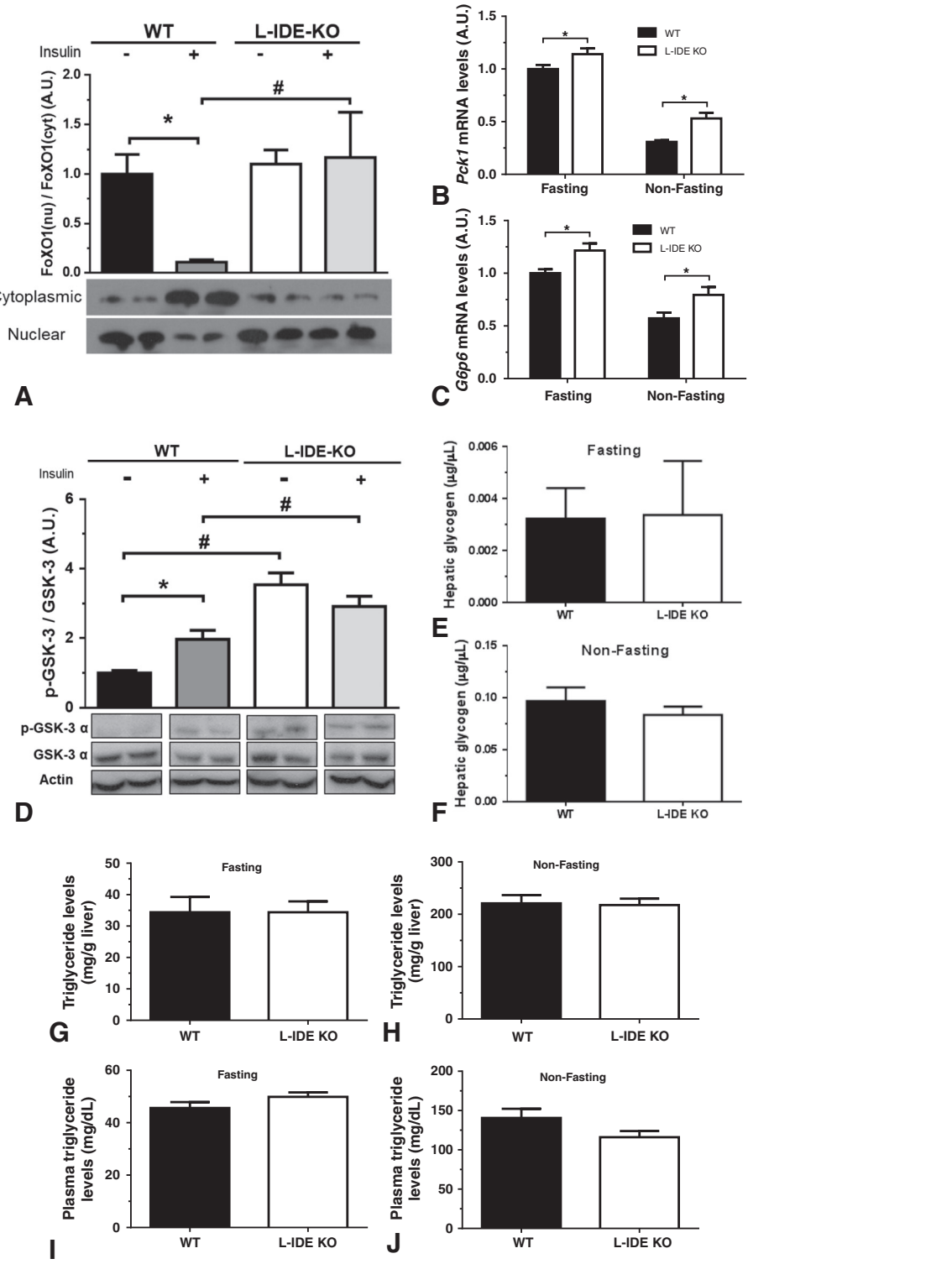

Fig. 6. Effects of *Ide* deletion on gluconeogenesis and glycogenesis. **(A)** Subcellular distribution of basal and insulin-stimulated FoxO1 in L-IDE-KO and WT mice. *Upper panel*: ratio of cytoplasmic vs. nuclear FoxO1 levels. *Lower panel*: representative image of cytoplasmic and nuclear fractions containing FoxO1. Data are mean ± SEM. $n = 4$ per genotype and condition. $^{*}p$ value <0.05 vs. saline treatment by ANOVA. $^{\#}p$ value <0.05 WT + insulin vs. L-IDE-KO + insulin treatment by ANOVA. Effects of *Ide* ablation on hepatic gluconeogenic gene expression. Livers from 3-month-old male L-IDE-KO and WT mice under fasting and non-fasting conditions were analyzed for mRNA levels of *Pck1* **(B)** and *G6pc* **(C).** Data are mean ± SEM. n = 3 in triplicate per genotype and condition. $^{*}p$ value < 0.05 vs. WT by Students' *t*-test. **(D, E, F)** Effects of *Ide* deletion on glycogenesis signaling. **(D)** *Upper panel*: densitometric analyses of GSK-3α. The *y*-axis represents the ratio of phosphorylated versus total protein in arbitrary units. *Lower panel*: representative western blots depicting basal and insulin-stimulated total and phosphorylated GSK-3α. Grouping of images from different parts of the same gel have been used for the final arrangement of the figure (see Supplementary Fig. 8 for full blots). Data are mean ± SEM. n = 6 per genotype and condition. $^{*}p$ value < 0.05 vs. saline treatment by ANOVA. $^{\#}p$ value < 0.05 WT vs. L-IDE-KO by ANOVA. Liver glycogen content under fasting **(E)** and non-fasting **(F)** conditions in 3-month-old male WT and L-IDE-KO mice. Data are mean ± SEM. n = 4 per genotype and condition. $^{*}p$ value < 0.05 vs. WT by Students' *t*-test. **(G, H, I, J)** Effects of *Ide* deletion on triglycerides levels. Hepatic triglycerides levels under fasting **(G)** and non-fasting **(H)** conditions in 3-month-old male WT and L-IDE-KO mice. Data are mean ± SEM. n = 4 per genotype and condition. Plasma triglycerides levels under fasting **(I)** and non-fasting **(J)** conditions in 3-month-old male WT and L-IDE-KO mice. Data are mean ± SEM. $n = 12$ per genotype and condition.

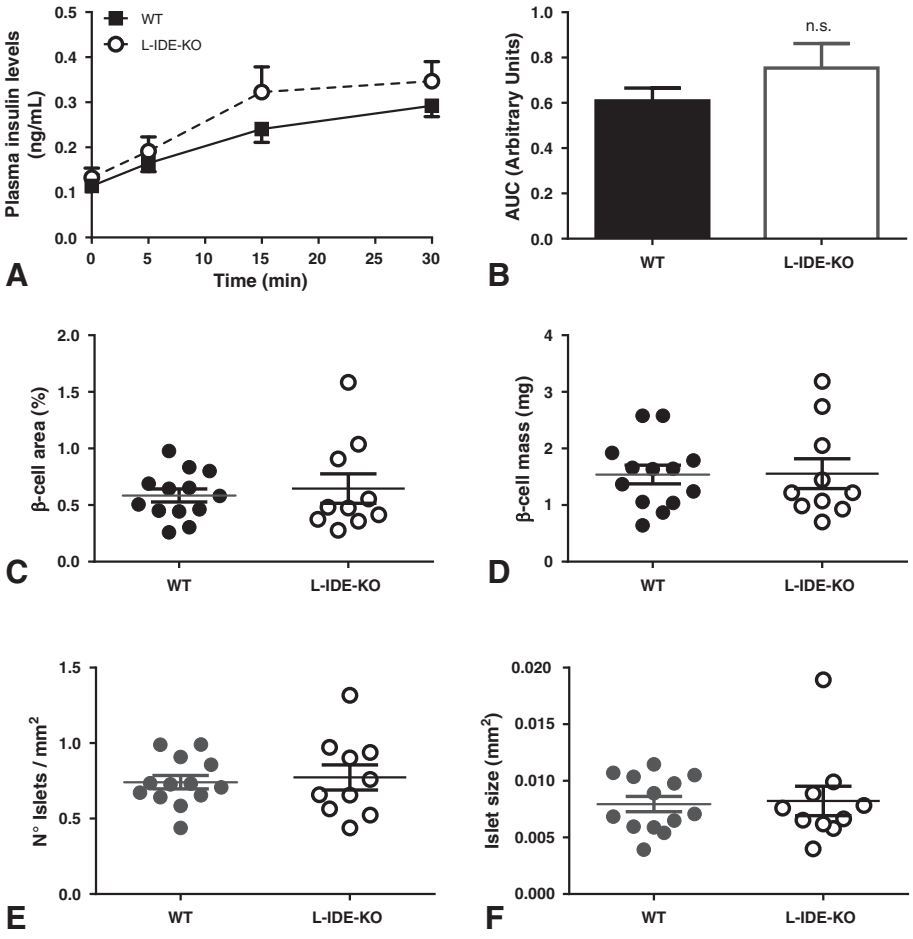

Fig. 7. Effects of *Ide* deletion on β-cell function and mass. **(A)** Plasma insulin levels during IP-GTT. Data are mean ± SEM. $n = 9$–13 per genotype and condition. **(B)** Area under the curve (AUC) of plasma insulin levels during the IP-GTT. n.s.; nonstatistical significance. Histomorphometry of pancreata. **(C)** β-cell area, **(D)** β-cell mass, **(E)** the number of islets, **(F)** the mean islets size. Data are mean ± SEM. $n = 10$–13 per genotype.

the number of islets, and the mean islets size were similar between both genotypes. Taken together these results indicate that β-cell function and mass are comparable in L-IDE-KO mice and WT mice.

4. Discussion

Using a mouse harboring liver-specific ablation of *Ide*, we show for the first time that hepatic deficiency of *Ide* does not result in hyperinsulinemia, as expected from deleting a protein that has been postulated to play a major role in hepatic insulin clearance. Extrahepatic tissues, such as kidneys, are also involved in insulin clearance in vivo, albeit to a lower extent than the liver [1]. However, IDE renal protein levels were not induced in L-IDE-KO mice to compensate for the loss of IDE in liver (Supplementary Fig. 9). Therefore, normoinsulinemia in L-IDE-KO mouse rules out a major role for IDE in hepatic insulin clearance. Consistently, Durham et al. demonstrated that NTE-1, an inhibitor of IDE, did not increase plasma insulin levels in rodents [16].

By excluding IDE as a significant mediator of insulin clearance in vivo, we postulate that other proteins might be more critical in this process. This could include CEACAM1, a substrate of the IR in liver that, upon its phosphorylation, promotes the uptake of the insulin-receptor complex and its targeting to the degradation process [9,10,38]. Hepatic loss-of-function of CEACAM1 by overexpressing its dominant-negative phosphorylation-defective isoform, reduced insulin clearance to cause hyperinsulinemia followed by secondary insulin resistance and impaired glucose tolerance [10]. CEACAM1 promotes insulin clearance by inducing the rate of insulin endocytosis via the less abundant, high-affinity isoform A of the IR (IR-A) [33]. Upon its phosphorylation on Tyr488 by the IR tyrosine kinase, via a mechanism requiring insulin-stimulated phosphorylation of the IR at Tyr1316, CEACAM1 recruits one or more molecules (including Shc) that bind to Tyr960 of the juxtamembrane domain of the IR to form a stable complex with the IR, and induce its uptake into clathrin-coated pits/vesicles [33]. Hence, CEACAM1 phosphorylation is required but not sufficient to allow receptor-mediated insulin endocytosis and degradation [33].

Our results demonstrate that in the absence of hepatic IDE, IR phosphorylation is decreased, but that of CEACAM1 is disproportionally abrogated. Thus, it is plausible that IDE participates in the internalization of the insulin-IR-CEACAM1 complex. Furthermore, hepatic depletion of IDE remarkably reduced insulin-stimulated association between Shc and CEACAM1, a critical step in the insulin's internalization process. It has been proposed that IDE is a multifunctional protein, which may perform unrelated functions as a scaffold protein involved in maintaining cellular homeostasis [39]. Whether such a proposed function of IDE is dependent on its protease activity, remains to be clarified. If IDE deletion completely blunts CEACAM1 phosphorylation (and function), one would question how is circulating insulin being removed in L-IDE-KO mice? First, CEACAM1 regulates insulin clearance by modulating insulin uptake via the less abundant IR-A isoform in the liver. The contribution of the more abundant IR-B isoform in insulin clearance in L-IDE-KO mice remains to be elucidated. Second, at physiological concentrations of the hormone, hepatic insulin clearance is mediated primarily by IR in the hepatocyte. However, the contribution of Kupffer cells to total insulin clearance in the liver is ~15%. Thus, it is possible that these cells compensate for the loss of insulin clearance in hepatocytes. Third, β-cell function and mass are similar between L-IDE-KO and control mice, suggesting that plasma insulin levels are

not related to changes in insulin secretion. Fourth, following insulin dissociation from its receptor in the acidic environment of the endosomes, insulin undergoes degradation whereas the receptor recycles to the plasma membrane. Thus, in the absence of IDE, insulin is carried back to the circulation bound to its receptor. Further research is needed to fully understand the process of intact hepatic insulin clearance in the L-IDE-KO mouse.

On the other hand, we showed that *Ide* deletion resulted in a significant ~30% reduction of the IR in the plasma membrane of hepatocytes from L-IDE-KO mice. Assuming that IDE does in fact degrade insulin in endosomes, depletion of IDE in hepatocytes might impair the removal of insulin and thereby impair the recycling of the IR to the cell surface. This scenario is in agreement with the observed effects of hepatic IDE depletion on plasma membrane IR levels in L-IDE-KO mice.

We herein demonstrate that ablation of hepatic *Ide* causes insulin resistance independently of circulating insulin levels. Our results partially coincide with those obtained by Farris et al. [12], and Abdul-Hay et al. [11] that showed a marked insulin resistance with increased chronic hyperinsulinemia in global IDE-KO mice. Systemic insulin resistance in these mice was hypothesized to emerge as a secondary compensatory response to chronic hyperinsulinemia. However, using the same IDE-KO mice, Miller et al. [40] and Steneberg et al. [41], reported normal plasma insulin levels in global IDE-KO mice. Nonetheless, our observations on L-IDE-KO mice suggest that the controversial systemic insulin resistance and glucose intolerance exhibited by IDE-KO mice are at least in part, a consequence of hepatic insulin resistance.

Whereas the liver-specific IR knockout mice (LIRKO) share with L-IDE-KO mice elevated plasma glucose levels, glucose intolerance and hepatic insulin resistance, they differ by developing chronic hyperinsulinemia in part, resulting from a failure to clear circulating insulin by receptor-mediated endocytosis [42,43]. This suggests that *Ide* deficiency per se causes insulin resistance and glucose intolerance independently of hyperinsulinemia. From this point of view, our data identify a role for IDE in the molecular pathways underlining hepatic insulin resistance, independently of their effect on glucagon, amylin and Aβ40.

In summary, L-IDE-KO mice provides an in vivo evidence that the absence of hepatic IDE causes insulin resistance, higher blood glucose levels, and glucose intolerance, through molecular mechanisms involving impaired hepatic insulin signaling and upregulation of gluconeogenic gene transcription. In agreement with previous studies [16], this appears to occur via a mechanism that does not implicate its role in hepatic insulin degradation. With the important caveat that non-proteolytic functions of IDE might be operative in the observed phenotype, these results suggest that pharmacological inhibition of IDE are contraindicated in the treatment of type 2 diabetes.

Supplementary data to this article can be found online at https://doi.org/10.1016/j.metabol.2018.08.001.

Authorship

ICC and GP contributed to conception and design of the work. PVP, CMFD, CDL, AM, BM, HEG, ICC, and GP make substantial contributions to acquisition, analysis, and interpretation of data. PVP and PC performed gene expression analyses. HTM and SMN performed western blots and analyses of CEACAM1 and co-IP experiments. ICC and GP participate in drafting the manuscript. HTM, SMN, MAL, ICC and GP participate in revising the manuscript critically for important intellectual content. The guarantors for the content of the article are Irene Cózar-Castellano and German Perdomo.

Conflict of Interest

We wish to confirm that there are no known conflicts of interest associated with this publication and there has been no significant financial support for this work that could have influenced its outcome. We confirm that the manuscript has been read and approved by all named authors and that there are no other persons who satisfied the criteria for authorship but are not listed. We further confirm that the order of authors listed in the manuscript has been approved by all co-authors.

Acknowledgments

We thank Prof. Henry Dong for providing us with the anti-FoxO1 antibody, and for critical reading of the manuscript and fruitful discussions.

The study was partially presented as a poster in the 53rd Annual Meeting of the European Association for the Study of Diabetes, Lisbon 2017.

Funding

This work was supported by grants from the Ministerio de Economía, Industria y Competitividad: SAF2014-58702-C2-1-R and SAF2016-77871-C2-1-R to ICC; SAF2014-58702-C2-2-R and SAF2016-77871-C2-2-R to GP; supported by the EFSD European Research Programme on New Targets for Type 2 Diabetes supported by an educational research grant from MSD to ICC and GP; the National Institutes of Health: R01-DK054254, R01-DK083850 and RO1-HL-112248 to SMN, and R01-GM115617 to MAL; and the American Diabetes Association: Career Development Award 7-11-CD-13 to MAL.

References

[1] Duckworth WC, Bennett RG, Hamel FG. Insulin degradation: progress and potential. Endocr Rev 1998;19:608–24.
[2] Shen Y, Joachimiak A, Rosner MR, Tang WJ. Structures of human insulin-degrading enzyme reveal a new substrate recognition mechanism. Nature 2006;443:870–4.
[3] Authier F, Posner BI, Bergeron JJ. Insulin-degrading enzyme. Clin Invest Med 1996;19:149–60.
[4] Bulloj A, Leal MC, Xu H, Castano EM, Morelli L. Insulin-degrading enzyme sorting in exosomes: a secretory pathway for a key brain amyloid-beta degrading protease. J Alzheimers Dis 2010;19:79–95.
[5] Farris W, Leissring MA, Hemming ML, Chang AY, Selkoe DJ. Alternative splicing of human insulin-degrading enzyme yields a novel isoform with a decreased ability to degrade insulin and amyloid beta-protein. Biochemistry 2005;44:6513–25.
[6] Akiyama H, Shii K, Yokono K, Yonezawa K, Sato S, Watanabe K, et al. Cellular localization of insulin-degrading enzyme in rat liver using monoclonal antibodies specific for this enzyme. Biochem Biophys Res Commun 1988;155:914–22.
[7] Duckworth WC. Insulin degradation: mechanisms, products, and significance. Endocr Rev 1988;9:319–45.
[8] Bevan P. Insulin signalling. J Cell Sci 2001;114:1429–30.
[9] Heinrich G, Ghadieh HE, Ghanem SS, Muturi HT, Rezaei K, Al-Share QY, et al. Loss of hepatic CEACAM1: a unifying mechanism linking insulin resistance to obesity and non-alcoholic fatty liver disease. Front Endocrinol 2017;8:8.
[10] Poy MN, Yang Y, Rezaei K, Fernstrom MA, Lee AD, Kido Y, et al. CEACAM1 regulates insulin clearance in liver. Nat Genet 2002;30:270–6.
[11] Abdul-Hay SO, Kang D, McBride M, Li L, Zhao J, Leissring MA. Deletion of insulin-degrading enzyme elicits antipodal, age-dependent effects on glucose and insulin tolerance. PLoS One 2011;6:e20818.
[12] Farris W, Mansourian S, Chang Y, Lindsley L, Eckman EA, Frosch MP, et al. Insulin-degrading enzyme regulates the levels of insulin, amyloid beta-protein, and the beta-amyloid precursor protein intracellular domain in vivo. Proc Natl Acad Sci U S A 2003;100:4162–7.
[13] Costes S, Butler PC. Insulin-degrading enzyme inhibition, a novel therapy for type 2 diabetes? Cell Metab 2014;20:201–3.
[14] Tang WJ. Targeting insulin-degrading enzyme to treat type 2 diabetes mellitus. Trends Endocrinol Metab 2016;27:24–34.
[15] Deprez-Poulain R, Hennuyer N, Bosc D, Liang WG, Enee E, Marechal X, et al. Catalytic site inhibition of insulin-degrading enzyme by a small molecule induces glucose intolerance in mice. Nat Commun 2015;6:8250.
[16] Durham TB, Toth JL, Klimkowski VJ, Cao JX, Siesky AM, Alexander-Chacko J, et al. Dual exosite-binding inhibitors of insulin-degrading enzyme challenge its role as the primary mediator of insulin clearance in vivo. J Biol Chem 2015;290:20044–59.
[17] Maianti JP, McFedries A, Foda ZH, Kleiner RE, Du XQ, Leissring MA, et al. Anti-diabetic activity of insulin-degrading enzyme inhibitors mediated by multiple hormones. Nature 2014;511:94–8.
[18] Cotsapas C, Prokunina-Olsson L, Welch C, Saxena R, Weaver C, Usher N, et al. Expression analysis of loci associated with type 2 diabetes in human tissues. Diabetologia 2010;53:2334–9.
[19] Fakhrai-Rad H, Nikoshkov A, Kamel A, Fernstrom M, Zierath JR, Norgren S, et al. Insulin-degrading enzyme identified as a candidate diabetes susceptibility gene in GK rats. Hum Mol Genet 2000;9:2149–58.
[20] Pivovarova O, Hohn A, Grune T, Pfeiffer AF, Rudovich N. Insulin-degrading enzyme: new therapeutic target for diabetes and Alzheimer's disease? Ann Med 2016;48:614–24.

[21] Duggirala R, Blangero J, Almasy L, Dyer TD, Williams KL, Leach RJ, et al. Linkage of type 2 diabetes mellitus and of age at onset to a genetic location on chromosome 10q in Mexican Americans. Am J Hum Genet 1999;64:1127–40.
[22] Elbein SC, Hoffman MD, Teng K, Leppert MF, Hasstedt SJ. A genome-wide search for type 2 diabetes susceptibility genes in Utah Caucasians. Diabetes 1999;48:1175–82.
[23] Postic C, Shiota M, Niswender KD, Jetton TL, Chen Y, Moates JM, et al. Dual roles for glucokinase in glucose homeostasis as determined by liver and pancreatic beta cell-specific gene knock-outs using Cre recombinase. J Biol Chem 1999;274:305–15.
[24] Jimenez-Palomares M, Ramos-Rodriguez JJ, Lopez-Acosta JF, Pacheco-Herrero M, Lechuga-Sancho AM, Perdomo G, et al. Increased Abeta production prompts the onset of glucose intolerance and insulin resistance. Am J Physiol Endocrinol Metab 2012;302:E1373–80.
[25] Perdomo G, Kim DH, Zhang T, Qu S, Thomas EA, Toledo FG, et al. A role of apolipoprotein D in triglyceride metabolism. J Lipid Res 2010;51:1298–311.
[26] Sanchez-Encinales V, Cozar-Castellano I, Garcia-Ocana A, Perdomo G. Targeted delivery of HGF to the skeletal muscle improves glucose homeostasis in diet-induced obese mice. J Physiol Biochem 2015;71:795–805.
[27] Ahren B, Thomaseth K, Pacini G. Reduced insulin clearance contributes to the increased insulin levels after administration of glucagon-like peptide 1 in mice. Diabetologia 2005;48:2140–6.
[28] Livak KJ, Schmittgen TD. Analysis of relative gene expression data using real-time quantitative PCR and the 2(−delta delta c(t)) method. Methods 2001;25:402–8.
[29] Qu S, Altomonte J, Perdomo G, He J, Fan Y, Kamagate A, et al. Aberrant Forkhead box O1 function is associated with impaired hepatic metabolism. Endocrinology 2006;147:5641–52.
[30] Russo L, Muturi HT, Ghadieh HE, Ghanem SS, Bowman TA, Noh HL, et al. Liver-specific reconstitution of CEACAM1 reverses the metabolic abnormalities caused by its global deletion in male mice. Diabetologia 2017;60:2463–74.
[31] Russo L, Muturi HT, Ghadieh HE, Wisniewski AM, Morgan EE, Quadri SS, et al. Liver-specific rescuing of CEACAM1 reverses endothelial and cardiovascular abnormalities in male mice with null deletion of Ceacam1 gene. Mol Metab 2018;9:98–113.
[32] Lopez-Acosta JF, Villa-Perez P, Fernandez-Diaz CM, Roman Dde L, Diaz-Marrero AR, Cueto M, et al. Protective effects of epoxypukalide on pancreatic beta-cells and glucose metabolism in STZ-induced diabetic mice. Islets 2015;7:e1078053.
[33] Najjar SM. Regulation of insulin action by CEACAM1. Trends Endocrinol Metab 2002;13:240–5.
[34] Poy MN, Ruch RJ, Fernstrom MA, Okabayashi Y, Najjar SM. Shc and CEACAM1 interact to regulate the mitogenic action of insulin. J Biol Chem 2002;277:1076–84.
[35] Kim DH, Zhang T, Ringquist S, Dong HH. Targeting FoxO1 for hypertriglyceridemia. Curr Drug Targets 2011;12:1245–55.
[36] von Wilamowitz-Moellendorff A, Hunter RW, Garcia-Rocha M, Kang L, Lopez-Soldado I, Lantier L, et al. Glucose-6-phosphate-mediated activation of liver glycogen synthase plays a key role in hepatic glycogen synthesis. Diabetes 2013;62:4070–82.
[37] Leavens KF, Easton RM, Shulman GI, Previs SF, Birnbaum MJ. Akt2 is required for hepatic lipid accumulation in models of insulin resistance. Cell Metab 2009;10:405–18.
[38] Deangelis AM, Heinrich G, Dai T, Bowman TA, Patel PR, Lee SJ, et al. Carcinoembryonic antigen-related cell adhesion molecule 1: a link between insulin and lipid metabolism. Diabetes 2008;57:2296–303.
[39] Tundo GR, Sbardella D, Ciaccio C, Grasso G, Gioia M, Coletta A, et al. Multiple functions of insulin-degrading enzyme: a metabolic crosslight? Crit Rev Biochem Mol Biol 2017;52:554–82.
[40] Miller BC, Eckman EA, Sambamurti K, Dobbs N, Chow KM, Eckman CB, et al. Amyloid-beta peptide levels in brain are inversely correlated with insulysin activity levels in vivo. Proc Natl Acad Sci U S A 2003;100:6221–6.
[41] Steneberg P, Bernardo L, Edfalk S, Lundberg L, Backlund F, Ostenson CG, et al. The type 2 diabetes-associated gene ide is required for insulin secretion and suppression of alpha-synuclein levels in beta-cells. Diabetes 2013;62:2004–14.
[42] Biddinger SB, Hernandez-Ono A, Rask-Madsen C, Haas JT, Aleman JO, Suzuki R, et al. Hepatic insulin resistance is sufficient to produce dyslipidemia and susceptibility to atherosclerosis. Cell Metab 2008;7:125–34.
[43] Michael MD, Kulkarni RN, Postic C, Previs SF, Shulman GI, Magnuson MA, et al. Loss of insulin signaling in hepatocytes leads to severe insulin resistance and progressive hepatic dysfunction. Mol Cell 2000;6:87–97.